Monthly Notices
of the
ROYAL ASTRONOMICAL SOCIETY

MNRAS **480,** 4183–4198 (2018)
Advance Access publication 2018 July 31

doi:10.1093/mnras/sty2047

Measuring the severity of close encounters between ringed small bodies and planets

Jeremy Wood,[1,2]★ Jonti Horner,[2,3] Tobias C. Hinse[4] and Stephen C. Marsden[2]

[1]*Hazard Community and Technical College, Community College Drive Hazard, KY 41701, USA*
[2]*Computational Engineering and Science Research Centre, University of Southern Queensland, West Street, Toowoomba, QLD 4350, Australia*
[3]*Australian Centre for Astrobiology, UNSW Australia, Sydney, NSW 2052, Australia*
[4]*Korea Astronomy and Space Science Institute, 776 Daedukdae-ro, Yuseong-gu, Daejeon 305-348, Republic of Korea*

Accepted 2018 July 20. Received 2018 June 21; in original form 2018 April 14

ABSTRACT

Rings have recently been discovered around the trans-Neptunian object (TNO) 136108 Haumea and the Centaur 10199 Chariklo. Rings are also suspected around the Centaur 2060 Chiron. As planetary close encounters with ringed small bodies can affect ring longevity, we previously measured the severity of such encounters of Chariklo and Chiron using the minimum encounter distance, $d_{\rm min}$. The value of $d_{\rm min}$ that separates noticeable encounters from non-noticeable encounters we called the 'ring limit', R. R was then approximated as 10 tidal disruption distances, $10R_{\rm td}$. In this work, we seek to find analytical expressions for R that fully account for the effects of the planet mass, small body mass, $m_{\rm s}$, ring orbital radius, r, and velocity at infinity, v_∞, for fictitious ringed Centaurs using ranges 2×10^{20} kg $\leq m_{\rm s} \leq 1$ Pluto mass and $25\,000 \leq r \leq 100\,000$ km. To accomplish this, we use numerical integration to simulate close encounters between each giant planet and ringed Centaurs in the three-body planar problem. The results show that R has a lower bound of approximately $1.8R_{\rm td}$. We compare analytical and experimental R values for a fictitious Haumea, Chariklo, and Chiron with $r = 50\,000$ km. The agreement is excellent for Haumea, but weaker for Chariklo and Chiron. The agreement is best for Jupiter and Saturn. The ring limits of the real Haumea, Chariklo, and Chiron are $<4R_{\rm td}$. Experimental R values for the fictitious bodies make better approximations for the R values of the real bodies than does $10R_{\rm td}$. Analytical values make good first approximations.

Key words: planets and satellites: dynamical evolution and stability – planets and satellites: rings – minor planets, asteroids: Individual:Chariklo – minor planets, asteroids: Individual:Chiron – minor planets, asteroids: Individual:Haumea.

1 INTRODUCTION

The Centaurs are a population of icy bodies moving on dynamically unstable orbits in the outer Solar system (e.g. Tiscareno & Malhotra 2003; Horner, Evans & Bailey 2004a,b; Di Sisto & Brunini 2007; Bailey & Malhotra 2009). The first Centaur discovered, 2060 Chiron, was found in 1977 (Kowal, Liller & Marsden 1979), and it was soon realized to be moving on a highly unusual orbit, spending almost all its time between the orbits of Saturn and Uranus. The second Centaur, 5145 Pholus, was found in 1992, and many more soon followed. The exact definition of a Centaur varies within the research community. This work defines Centaurs as objects with semimajor axes between the orbits of Jupiter and Neptune, and perihelia beyond Jupiter (e.g. Sheppard et al. 2000). Using this definition, more than 220 of these objects have been discovered.[1] It is the general consensus that Centaurs were perturbed into their present orbits via gravitational interactions with the giant planets. The original source of the Centaurs is thought to be the various stable small body populations of the outer Solar system. Through the years, a number of those populations have been put forward as potential contributors to the Centaurs, including the Edgeworth–Kuiper belt objects (e.g. Levison & Duncan 1997; Horner et al. 2004a), scattered disc objects (e.g. Di Sisto & Brunini 2007; Volk & Malhotra 2008), Oort cloud objects (e.g. Emel'yanenko, Asher & Bailey 2005; Brasser et al. 2012; Fouchard et al. 2014), Trojan asteroids of Jupiter (e.g. Horner & Evans 2006; Horner, Müller & Lykawka 2012b), and Trojan asteroids of Neptune (Horner & Lykawka 2010a,b; Horner et al. 2012a). On time-scales comparable

★ E-mail: jeremy.wood@kctcs.edu

[1] http://www.minorplanetcenter.net/iau/lists/Unusual.html (accessed 2016 January 15).

Table 1. The relevant orbital and physical properties of Chariklo, Chiron, and Haumea. The orbital data are based on observational arc lengths of 10 540.2, 44 773.2, and 22 795 d, respectively. The epoch is 58000.0 MJD. The mass range for Chiron was found using its density and radius ranges assuming a spherical shape. Ref: [1] = Leiva et al. (2017); [2] = Meech & Svoren (2004); [3] = Groussin, Lamy & Jorda (2004); [4] = Sykes & Walker (1991); [5]= Lacerda & Jewitt (2007); [6]= Rabinowitz et al. (2006); and [7] = Ragozzine & Brown (2009).

Body	Property	Value	Ref
Chariklo			
	Density	796–970 kg m^{-3}	[1]
	Mass	6×10^{18}–8×10^{18} kg	[1]
Chiron			
	Density	500–1000 kg m^{-3}	[2]
	Mass	7.50×10^{17}–2.70×10^{19} kg	–
	Radius	71 ± 5–186 km	[3], [4]
Haumea			
	Density	2600 kg m^{-3}	[5], [6]
	Mass	$4.006 \pm 0.040 \times 10^{21}$ kg	[7]

Table 2. The properties of the rings (or supposed rings) of Chariklo, Chiron, and Haumea. Ref: [1] = Braga-Ribas et al. (2014); [2] = Ortiz et al. (2015); and [3] = Ortiz et al. (2017).

Object	Inner ring (km)	Outer ring (km)	Widths (km)	Ref
Chariklo	390.6 ± 3.3	404.8 ± 3.3	7.17 ± 0.14; 3.4 + 1.1–1.4	[1]
Chiron	324	–	10	[2]
Haumea	2287	–	70	[3]

to the age of the Solar system (4.6 Gyr), Centaurs are indeed an ephemeral class of object, with dynamical lifetimes on the order of 10 Myr (Tiscareno & Malhotra 2003). Objects in the Centaur population typically experience frequent close encounters with the four giant planets. These encounters can drive rapid evolution of Centaur orbits on time-scales of just hundreds or thousands of years (Wood et al. 2017). This results in the orbits of Centaurs being chaotically perturbed, redistributing the objects throughout the Solar system, and in many cases, transferring them to other Solar system small body populations, such as the Jupiter-family comets (e.g. Tiscareno & Malhotra 2003). In addition to potentially being injected into the Jupiter-family comet population, the Centaurs face a variety of potential fates, including planetary collision, collision with the Sun, injection into the Oort cloud, or ejection from the Solar system. Centaurs may even enter the inner Solar system to threaten the inner planets (Napier 2015; Galiazzo, Wiegert & Aljbaae 2016; Araujo et al. 2018) or temporarily enter the scattered disc (e.g. Tiscareno & Malhotra 2003; Horner et al. 2004a,b; Bailey & Malhotra 2009). Given the dynamically chaotic nature of the Centaur region, it came as a complete surprise when two narrow rings were discovered around the largest Centaur Chariklo by means of a stellar occultation event in 2013 (Braga-Ribas et al. 2014). Analysis of occultation data concluded that the rings have radii of 391 and 405 km, with widths of about 7 and 3 km, respectively (Braga-Ribas et al. 2014). It has been suggested that rings may also exist or have existed around the Centaur Chiron (e.g. Ortiz et al. 2015; Pan & Wu 2016); satellites of Saturn and Uranus; and even the dwarf planet Pluto (Rawal & Nikouravan 2011; Sicardy et al. 2016). Whilst none of these have been definitively confirmed, the trans-Neptunian dwarf planet Haumea, which is known to have experienced a significant collisional disruption in the past, was recently found to have its own suite of rings (Ortiz et al. 2017), and it seems likely that, in the coming years, more ringed objects will be discovered. The relevant physical properties of Chariklo, Chiron, and Haumea along with those of their rings are shown in Tables 1 and 2. When considering the origin of the rings of the Centaurs, and whether or not they truly predate the injection of the objects to the Centaur population, it is relevant to note that the rings of Haumea are particularly interesting since Haumea is the largest object in the trans-Neptunian region's only known collisional family (e.g. Brown et al. 2007; Lykawka et al. 2012) – in other words, Haumea and its associated family are the debris left behind from a collision that could readily have injected material into orbits that would one day evolve to enter the Centaur population. Indeed, by integrating over 35 000 clones backwards in time, Wood et al. (2017, 2018) confirm that any rings around Chariklo or Chiron could predate their entrance into the Centaur region (Araujo, Sfair & Winter 2016). Once there, given the frequency with which the Centaurs experience close encounters with the giant planets, it is natural to wonder what effect such encounters would have on the rings around those objects. This has been investigated for the case of Chariklo by Araujo et al. (2016) in the seven-body (Sun, Chariklo, four giant planets, and ring particle) non-planar problem who stated that the effect of a close encounter on a ring was qualitatively 'noticeable' if the maximum change in eccentricity, $\Delta e_{\max}$, of the orbit of any ring particle starting in a circular orbit was $\geq$0.01. In that study, ring particles were initially randomly distributed in circular equatorial orbits with radii in the range 200–1000 km incremented in intervals of 20 km with 100 ring particles per orbit before the encounter. After the encounter, the minimum approach distance of the small body to the planet (the close encounter distance) and the largest change in eccentricity of the orbit of a ring particle were recorded. In this manner, those authors were able to investigate the likelihood that Chariklo's rings could survive through the duration of its life in the Centaur region. By studying the evolution of rings around 729 clones of Chariklo, they found that, in the majority (93 per cent) of cases, the rings remained unperturbed throughout the object's lifetime. In general, the encounter severity is related to the minimum approach distance, $d_{\min}$, between the ringed body and the planet. In Wood et al. (2017), a severity scale was introduced for close encounters between a ringed small body and a planet by comparing $d_{\min}$ to the critical distances of the Roche limit, tidal disruption distance, Hill radius, and a new quantity called the 'ring limit'. The ring limit was loosely defined as the upper limit on the value of $d_{\min}$ for close encounters between Chariklo and a giant planet that had a noticeable effect on a ring. This ring limit was set to a crude constant value of 10 tidal disruption distances based on the work of Araujo et al. (2008) as it may be related to the radius of the sphere of influence and the capture radius in the three-body problem. But this constant value ignores velocity effects. In this work, we seek to find analytical solutions for the ring limit in the three-body planar problem (small body, planet, and ring particle) that yield more accurate values than our current value of 10 tidal disruption distances. We use the technique of numerical integration to simulate close encounters between fictitious one-ringed bodies and each of the giant planets. In this manner, we determine the ring limit for Centaurs moving on hyperbolic and parabolic orbits around the planet. We derive analytical expressions for the ring limit as a function of small body mass, planet mass, ring orbital radius, and velocity at infinity of the Centaur's orbit about the planet in the three-body problem. We then use these expressions to analytically determine ring limits for fictitious Centaurs with

the masses of Chariklo, Haumea, and Chiron. Then the ring limits of these three fictitious bodies are experimentally determined via direct simulation and compared to their analytical values. Finally, we compare analytical ring limit values for a fictitious Chariklo to $d_{\min}$ values for planetary close encounters for a real Chariklo in the seven-body non-planar problem (Sun, four giant planets, Chariklo, and ring particle). This paper is partitioned as follows: in Section 2 we describe the properties of Chariklo, Chiron, and Haumea along with their rings; in Section 3 present the theory of close encounters; in Section 4 describe our experimental method; in Section 5 present our results; and summarize our conclusions in Section 6.

2 THE PROPERTIES OF CHARIKLO, CHIRON, HAUMEA, AND THEIR RINGS

The relevant physical properties of Chariklo, Chiron, and Haumea are shown in Table 1. The mass range of Chiron was calculated using its radius and density ranges assuming a spherical body. In the case of Haumea, the mass was determined using a model of Haumea with its two satellites.

The properties of the rings of Chariklo, Chiron, and Haumea are shown in Table 2.

3 THE THEORY OF CLOSE ENCOUNTERS

3.1 Determining the velocity at infinity of the orbit of the small body

Given the growing number of small Solar system bodies found to have rings, it is interesting to consider the effect of close encounters between those objects and the giant planets on their ring systems. How close must an encounter be before the influence of the planet on a ring is noticeable? One solution to this problem would be to carry out exhaustive *N*-body dynamical studies for every object found to have rings (such as those detailed in Wood et al. 2017, 2018). However, should many such objects be discovered, such simulations would eventually prove prohibitive, given their computationally intensive nature. It is therefore important to examine whether it is possible to develop a criterion by which the stability (or otherwise) of small body rings can be assessed, in the context of the close encounters they will experience throughout their lifetimes. Previously we built such a criterion in Wood et al. (2017) that was based entirely upon the idea that the severity of a given encounter is determined by the strength of the tidal effects on the small body's ring system. Thus, the severity only depended on the distance of the closest approach between the planet and Centaur, $d_{\min}$. However, the severity also depends on the velocity at infinity, v_∞, of the small body relative to the planet. v_∞ has little meaning for an elliptical orbit, however, in the overwhelming majority of cases, a small body undergoing a close encounter with a giant planet will follow a parabolic or hyperbolic path with respect to that planet, rather than being captured by it. For this reason, we therefore consider just parabolic and hyperbolic orbits in this work. If the orbit of the small body relative to the planet is parabolic or hyperbolic, then for a given planet and small body mass in the planar problem, the orbit is defined by v_∞ and $d_{\min}$. Hyodo et al. (2016) show the derivation of v_∞ for the case in which the planet is restricted to a circular orbit about the Sun in this planar three-body problem. The reader is referred to that work for details. Given a small body and a planet both in orbit about the Sun and having a close encounter, the resulting equations are

$$v_\infty^2 = v_r^2 + (v_\omega - v_{\rm K})^2, \tag{1}$$

where v_r and v_ω are the radial and azimuthal velocities, respectively, of the small body at the orbital distance of the planet from the Sun; and $v_{\rm K}$ is the Keplerian velocity of the planet in its orbit about the Sun. v_r and v_ω are given by

$$v_r = v_{\rm K}\sqrt{2 - \frac{a_{\rm o}}{a} - \frac{a(1-e^2)}{a_{\rm o}}}, \tag{2}$$

$$v_\omega = v_{\rm K}\sqrt{\frac{a(1-e^2)}{a_{\rm o}}}, \tag{3}$$

where a is the semimajor axis of the orbit of the small body, $a_{\rm o}$ is the semimajor axis of the orbit of the planet, and e is the eccentricity of the orbit of the small body about the Sun.

3.2 Critical distances and the ring limit

We define the ring limit, R, as the value of the minimum approach distance for close encounters between a planet and a ringed small body in a hyperbolic or parabolic orbit about the planet in the three-body planar problem for which the effect on the ring is just noticeable following the criterion of Araujo et al. (2016) for a just-noticeable encounter. The ring limit then defines a boundary between a noticeable and non-noticeable effect. This makes R distinct from the Hill radius, $R_{\rm H}$, tidal disruption distance, $R_{\rm td}$, and Roche limit, $R_{\rm roche}$, as each of these involves a balance of forces. For reason of comparison, it is beneficial to discuss these critical distances in more detail. The Hill radius of a less massive body with respect to a more massive body can be defined as the distance from the less massive body within which a satellite may orbit. If the satellite orbit is within the Hill radius, then the less massive body–satellite binary cannot be disrupted by tidal forces due to the more massive body. In the case for which the more massive body is a planet and the less massive body a small body of the Solar system, the Hill radius of the small body with respect to the planet is approximately given by

$$R_{\rm H} \approx R_{\rm radial}\left(\frac{m_{\rm s}}{3M_{\rm p}}\right)^{\frac{1}{3}} \tag{4}$$

(e.g. Murray & Dermott 1999), where $m_{\rm s}$ is the mass of a small body, $M_{\rm p}$ the mass of the planet, and $R_{\rm radial}$ the radial distance between the small body and the planet. Thus, during a close encounter between a ringed small body and a planet, the distance of orbiting ring particles from the small body must be less than that small body's Hill radius with respect to the planet in order for the ring particles to remain in orbit. Analogously the satellite of a planet must remain within the planet's Hill radius with respect to the Sun. It should be noted that equation (4) neglects velocity effects. In the three-body problem (central body, planet small body), when the small body has a close encounter with the planet, if the initial relative velocity of the encounter, $v_{\rm rel}$, is accounted for, then two critical distances are of interest. First, the influence radius, $R_{\rm inf}$, is that distance between the small body and planet at which the gravitational effect of the planet on the small body alters the two-body energy of the small body relative to the central body by 1 per cent. Second, the capture radius, $R_{\rm cap}$, is the distance between the small body and planet within which the small body is captured into a Keplerian orbit about the planet (or the two-body small body–planet energy is negative) even if just temporarily. Both $R_{\rm inf}$ and $R_{\rm cap}$ are functions of the mass

ratio of the small body to the planet, μ_2, and $v_{\rm rel}$. For example, for the range $2 \times 10^{-8} \leq \mu_2 \leq 2 \times 10^{-6}$, $R_{\rm inf}$ is given in units of Hill radii by

$$R_{\rm inf} = 1.00 - (2.48 \times 10^{-10})\mu_2^{-2.60-0.14\log(\mu_2)} v_{\rm rel}, \quad (5)$$

and for the range $\mu_2 < 2 \times 10^{-8}$, $R_{\rm inf}$ lies within 0.5 Hill radius. For the range $10^{-12} \leq \mu_2 \leq 10^{-1}$, $R_{\rm cap}$ is approximated in units of Hill radii by

$$R_{\rm cap} \approx 1.2 - 0.35\mu_2^{0.32} v_{\rm rel} \quad (6)$$

(Araujo et al. 2008).

At a closer distance to the planet lies the tidal disruption distance. If a ringed small body is at a distance just within the tidal disruption distance from a planet, tidal forces can disrupt a small body–ring particle binary pair instantaneously. The tidal disruption distance for a binary consisting of a small body and a massless ring particle in a circular orbit of radius r about the small body is given by

$$R_{\rm td} \approx r\left(\frac{3M_{\rm p}}{m_{\rm s}}\right)^{\frac{1}{3}} \quad (7)$$

(Agnor & Hamilton 2006; Philpott, Hamilton & Agnor 2010). For example, when Chariklo is just within the tidal disruption distance to a planet, a ring particle is just outside Chariklo's Hill radius with respect to the planet. There is one more critical distance to consider. At an even closer distance to a planet is the Roche limit – the distance from a more massive body (the primary body) within which a much less massive body (the secondary body) held together only by gravity can be torn apart by tidal forces. For a rigid secondary body, the equation for the Roche limit with respect to a primary body is approximately

$$R_{\rm roche} \approx 1.44 R_{\rm p}\left(\frac{\rho_{\rm p}}{\rho_{\rm s}}\right)^{\frac{1}{3}}, \quad (8)$$

where $R_{\rm p}$ is the physical radius of the primary body, $\rho_{\rm p}$ is the density of the primary body, and $\rho_{\rm s}$ is the density of the secondary body (e.g. Jeans 1928; Jeffreys 1947; Murray & Dermott 1999). To give the reader a feel for the relative scale of these three parameters, we calculate the Hill radius of a planet with respect to the Sun, tidal disruption distance, and Roche limit using a Chariklo mass of 8×10^{18} kg (Leiva et al. 2017) and ring orbital radius set to that of the outer ring of Chariklo of 405 km for each of the four giant planets. The Roche limits of Chariklo with respect to each giant planet were calculated for the case in which the density of Chariklo is 970 kg m^{-3} (Leiva et al. 2017). Planetary data were obtained from the NASA JPL HORIZONS ephemeris.[2] The results are shown in Table 3.

We now present in Table 4 our previously developed severity scale for a close encounter between a ringed small body and a planet based on the value of $d_{\rm min}$ relative to the Hill radius of the planet with respect to the Sun, ring limit, tidal disruption distance, and Roche limit. Here, our aim is to define a more accurate/refined ring-limit distance resulting in a more rigorous quantitative close encounter severity scale in the planar three-body problem. In our previously published scale for the seven-body problem, only a constant value of 10 tidal disruption distances was used for the ring limit (Wood et al. 2017).

[2]http://ssd.jpl.nasa.gov/horizons.cgi?s_body=1#top (accessed 2015 December 31) for epoch 2000 January 1, at 0:00UT. The NASA ephemeris system was created by Jon Giorgini.

Table 3. Approximate Roche limits, tidal disruption distances, and Hill radii for Chariklo for the four giant planets using a Chariklo mass of 8×10^{18}kg, density equal to 970 kg m^{-3}, and a ring orbital radius of 405 km. Hill radii were calculated for each giant planet with respect to the Sun.

Planet	Roche limit (km)	Tidal disruption distance (km)	Hill radius (km)
Jupiter	114 256	362 000	5.30×10^7
Saturn	77 359	242 000	6.52×10^7
Uranus	40 765	129 000	6.99×10^7
Neptune	42 468	137 000	1.16×10^8

Table 4. A scale ranking the close encounter severity between a ringed small body and a planet based on the minimum distance obtained between the small body and the planet, $d_{\rm min}$, during the close encounter taken from Wood et al. (2017). $R_{\rm H}$, R, $R_{\rm td}$, and $R_{\rm roche}$ are the Hill radius of the planet with respect to the Sun, ring limit, tidal disruption distance, and Roche limit, respectively. For that work, the ring limit was set to a constant value of 10 tidal disruption distances.

$d_{\rm min}$ range	Severity
$d_{\rm min} \geq R_{\rm H}$	Very low
$R \leq d_{\rm min} < R_{\rm H}$	Low
$R_{\rm td} \leq d_{\rm min} < R$	Moderate
$R_{\rm roche} \leq d_{\rm min} < R_{\rm td}$	Severe
$d_{\rm min} < R_{\rm roche}$	Extreme

Unlike the other critical distances, no simple equation for R is available. We expect that R should be a function of planet mass, small body mass, relative small body velocity at infinity, and ring orbital radius. This would be a five-dimensional problem. However, if any two of the five quantities are held constant, the problem becomes one in only three dimensions. One example of this would be to hold the planet mass and small body mass constant while varying the other variables. We theorize that the mathematical form of an equation for R in this three-dimensional (3D) problem can be written as a factor f of the tidal disruption distance:

$$R = f R_{\rm td} = f r\left(\frac{3M_{\rm p}}{m_{\rm s}}\right)^{\frac{1}{3}}, \quad (9)$$

where $f > 1$. This is justified because the impact of an encounter on the ring will become noticeable at a greater distance than that at which the orbit of a ring particle would be completely disrupted. We expect f to be a function of the orbital radius, velocity at infinity, mass of the small body, and mass of the planet. Thus, $f = f(r, v_\infty, m_{\rm s}, M_{\rm p})$. f is dimensionless but can be thought of as the value of the ring limit expressed in units of tidal disruption distances. For close encounters with any particular planet, $M_{\rm p}$ is constant, and this problem can be simplified even further by holding any two of the variables r, v_∞, and $m_{\rm s}$ constant. Given these variables, we can use numerical integrations to quantify the value of f, and therefore work towards a standard formulism for the ring limit.

4 NUMERICAL METHOD

As the three- – or more – body problem cannot be solved analytically, computers have been used to numerically approximate such systems using integration. Over the decades, computing power has continued to increase allowing for more and more robust simulations in areas such as Solar system dynamics, exoplanets, star clusters, and even galactic astronomy (Horner & Jones 2010; Wang

et al. 2015; Benson, Cannella & Cole 2016; Horner & Wittenmyer 2018). In this work we make use of a relatively new integrator in an attempt to find specific analytical solutions for the ring limit.

4.1 Initializing the simulations

In order to explore the complicated five-parameter problem in three dimensions, we used the technique of numerical integration of the three-body planar problem (small body, giant planet, and ring particle) to simulate close encounters between giant planets and small one-ringed bodies in hyperbolic or parabolic orbits about a planet. Before any integration could be made, quantities such as initial distance and time step needed to be determined. To accomplish this, dozens of pre-runs were made in the three-body problem using the IAS15 integrator in the REBOUND *N*-body simulation package (Rein & Liu 2012; Rein & Spiegel 2015). Based on the results from these pre-runs it was decided that an adaptable time step of 0.001 yr would be used that would automatically adjust itself during the event of a close encounter. Determining the initial distance of a small body from a planet is tricky. If the initial distance chosen is too close, then the close encounter is too brief to noticeably alter the orbit of a ring particle when otherwise it would. If the initial distance chosen is too large, then much computation time is wasted as the small body makes it way toward the planet. After a significant amount of benchmarking, we chose to begin our simulations with the ringed small body located one Uranus Hill radius away from Jupiter, Saturn, and Uranus. For Neptune, the ringed small body began the simulation at a distance of one Neptune Hill radius from the giant planet. These initial conditions represented the optimal compromise between the length of arc on a given encounter and the amount of computational time required for the simulations. It was decided that a simulation would be terminated after the planet–small body distance went beyond the initial distance after the close encounter occurred. Following Hyodo et al. (2016) the range for v_∞ was found using orbital parameters of fictitious Centaurs, namely those with semimajor axes between Jupiter and Neptune with eccentricities in the range $e \leq 0.9$. The velocity at infinity ranges were found for all four giant planets using the equations in Section 3. It was found that the range of $0 \leq v_\infty \leq 9$ km s^{-1} overlapped the range for each planet so this range was chosen for our study. The v_∞ values were found by combining two sets. The first set was found by incrementing the range $0 \leq v_\infty \leq 9$ km s^{-1} in 0.25 km s^{-1} intervals. The second set was found by incrementing the range $0.9 \leq v_\infty \leq 8.9$ km s^{-1} in 1 km s^{-1} intervals. This particular range is arbitrary, but is broad enough to allow for an exploration of the dependence of the ring limit on the velocity at infinity. For the small body mass range, we wanted a range that allowed the dependence of the ring limit on small body mass to be fully explored and included masses large enough to retain rings. It was decided that the small body masses would range from just above the mass of Chariklo to the mass of Pluto. The range chosen was $2 \times 10^{20} \leq m_s \leq 1.309 \times 10^{22}$kg (the mass of Pluto)[3] which includes the mass of Haumea but not Chiron or Chariklo. We consider this mass range to be in the realm where $M_p \gg m_s$ as the planet masses are $>10^6$ times larger than any small body mass in the range. The mass range was incremented as follows. First, the mass of Pluto was used. Then for the range $1 \times 10^{21} \leq m_s \leq 9 \times 10^{21}$ kg masses were partitioned in increments of 1×10^{21} kg. Finally, for the range $2 \times 10^{20} \leq m_s \leq 9 \times 10^{20}$ kg masses were partitioned in increments of 1×10^{20} kg. This particular mass range is arbitrary and is a result of a compromise between desired masses and computation speed. It falls within the range studied by Araujo et al. (2008) and is large enough that the behaviour of the ring limit as a function of m_s can be fully explored. This range overlaps the mass of the ringed trans-Neptunian object (TNO) Haumea. It is widely established that TNOs can evolve to become Centaurs (e.g. Duncan, Levison & Dones 2004; Horner et al. 2004a; Di Sisto & Brunini 2007; Wood et al. 2017, 2018), and also that many TNOs may well have originated in the Centaur region, during the process of planet formation. As a result, it is clearly of interest to consider a range of masses that includes that of the known objects in trans-Neptunian regions, as it seems likely that, either in the past or the future, close encounters between ringed bodies of such mass and the giant planets may well have occurred. When choosing a range for the ring orbital radii, we wanted a range large enough that the dependence of the ring limit on r could be fully explored but small enough so that the rings would lay well within the Hill radius of the small body with respect to the Sun. It was decided that a range of $30\,000$ km $\leq r \leq 100\,000$ km would be used for these simulations. Through that range, we sampled at increments of 5000 km. In addition, we performed extra simulations for Saturn ($r = 25\,000$ km) and Jupiter ($r = 36\,000$, $42\,000$, $44\,000$, $46\,000$, and $48\,000$ km) in order to help us better characterize the behaviour of rings for encounters with those planets. This particular range is arbitrary and is the result of a compromise between desired values and computation time. However, the range is large enough that the behaviour of the ring limit as a function of r can be fully explored. We decided that a total of 100 massless test particles would be used to simulate the ring if $r < 50\,000$ km, and 500 massless test particles would be used if $50\,000 \leq r \leq 100\,000$ km. It was decided that these numbers of test particles worked best based on results from the pre-runs. For example, for r values in the range $50\,000 \leq r \leq 100\,000$ km it was found that changing the number of ring particles from 500 to 1000 did not have a significant effect on the values of the ring limits determined, so using only 500 particles was good enough. In each simulation, the ring particles were initially evenly distributed throughout the same circular orbit about the small body.

4.2 Determining the ring limit

To determine a ring limit value for any set of values of m_s, r, v_∞, and the mass of the planet in question, a close encounter between the small body and planet was simulated starting with the previously described initial conditions and an initial guess at the value of d_{min}. After the simulation, Δe_{max} was then determined from the simulation output. If $\Delta e_{max} = 0.01$, then d_{min} is equal to the ring limit. To numerically approximate this, a tolerance, ϵ, was used such that if $|\Delta e_{max} - 0.01| < \epsilon$, then the ring limit was set equal to d_{min} and recorded in units of both kilometres and tidal disruption distances. If however $|\Delta e_{max} - 0.01|$ was not within this certain tolerance, then the close encounter was run again with d_{min} increased/decreased if $\Delta e_{max} - 0.01$ was positive/negative. This process was continued until $|\Delta e_{max} - 0.01|$ was within the certain tolerance. The tolerances used were 1×10^{-5} if $R_{td} > 1000\,000$ km and 1×10^{-4} otherwise. The use of these different tolerances made R accurate to within 1000 km in each case. For each value of r used for each small body mass, 46 measurements of R were made each using a different value of velocity at infinity chosen from the range $0 \leq v_\infty \leq 9$ km s^{-1} partitioned as previously described.

[3] http://solarsystem.nasa.gov/planets/pluto/facts (accessed 2017 February 19).

4.3 The ring limit in three dimensions

To determine an analytical solution for the ring limit, we needed to discover the mathematical relationship between the ring limit and each of the four variables – small body mass, planet mass, ring orbital radius, and velocity at infinity. Our strategy was to hold two variables constant, plot our data in 3D phase space to create 3D structures and then use two-dimensional (2D) slices of those structures while holding a third quantity constant to determine the mathematical relationship between the ring limit and the fifth variable. Two major sets of integrations were performed – one with the small body mass held constant and the other with the ring orbital radius held constant. Then for each major integration, the data were analysed by holding the planet mass constant. In this way, 3D structures were created from the data of each major integration.

4.3.1 The ring limit as a function of velocity at infinity, ring orbital radius, and planet mass

In the first set of major integrations, we held the mass of the small body constant by setting it equal to the mass of Pluto (we will henceforth refer to a small body with the mass of Pluto as a Pluto-like body). Next, the mass of the planet was held constant and then the integrations were performed. This was done for each giant planet, and the data from those integrations were used to create four 3D structures in R–r–v_∞ space. Up to 20 values of r and 46 values of v_∞ were chosen from the previously described ranges. The number of simulations totalled between 700 and 920 per planet. In our initial simulations, we were unsure of how many would be needed to obtain a clear result. After several trials, it was realized that 700 simulations per scenario were sufficient to give an accurate value, and all future trials were run in this manner. The data from the extra simulations carried out in our earliest work were kept, which explain those cases where up to 920 simulations were carried out.

4.3.2 The ring limit as a function of small body mass and velocity at infinity

Another major set of integrations was performed with the ring orbital radius set to a constant value of 50 000 km and the mass of the planet set to the mass of Jupiter. It was not necessary to extend these integrations to every planet since planet mass was varied in the other previously mentioned major set of integrations. Using data from these integrations, a 3D structure in R–m_s–v_∞ space was created.

4.4 The ring limit in two dimensions

The ring limit can be studied in two dimensions by using 2D slices of 3D structures while holding a third variable constant everywhere in the slice. The ring limit's dependence on the planet mass was found by combining all four 3D structures in R–r–v_∞ space into one superstructure. Then the intersection of 2D slices of constant ring orbital radius and velocity at infinity allowed the planet mass dependence to be determined. 2D slices of R–r–v_∞ structures were made for each planet using a constant value of v_∞ and planet mass for each slice. Within each slice, R varied only with r. Then for each slice, a regression was done on R and r values to determine the best-fitting curve. This was done for each of the 46 different slices per r per planet. 2D slices of each R–r–v_∞ structure were also made using a constant value of r and planet mass for each slice. Within each slice, R varied only with v_∞. Then for each slice, a regression was done on R and v_∞ values to determine the best-fitting curve. Up to 20 different 2D slices of constant r were made per planet. Using an analogous technique, 2D slices of our plot in R–m_s–v_∞ space were made using a constant value of planet mass along with either a constant m_s or v_∞ for each slice. Each slice was studied using regression. 18 slices were made with a constant m_s and 46 with a constant v_∞ for each m_s value. The entire analysis plan is shown in Fig. 1.

4.5 Testing the analytical solutions

To test our analytical solutions, the ring limits for fictitious Centaurs with the masses of Chariklo, Haumea, and Chiron and a ring orbital radius of 50 000 km were found for the case $v_\infty = 9$ km s^{-1} via direct simulation. This particular value of v_∞ was selected because it always yielded the largest ring limit value for any particular small-body–planet encounter. Ring limit values for these three bodies in this case were also found analytically. Then the experimental values were compared to their analytical counterparts for agreement. Finally, we compared our analytical solutions over the entire range $0 \leq v_\infty \leq 9$ km s^{-1} to $d_{\min}$ values reported by Araujo et al. (2016) for the seven-body non-planar problem to see if our analytical solutions could be used collectively as an upper bound on the ring limit for Chariklo.

5 RESULTS

5.1 The ring limit in three dimensions

Fig. 2 shows examples of plots of our data in R–r–v_∞ space for each planet for close encounters with a Pluto-like body. Fig. 3 shows the same 3D graphs in a rotated view for all planets on one plot with different colours being used for each planet. A series of islands of data points can be seen for each planet. The effect of planet mass on the ring limit can clearly be seen. Given a constant velocity at infinity and ring orbital radius, the ring limit increases with planet mass. This result is not surprising. We know that a planet with a larger mass has a stronger gravitational pull than a planet with a smaller mass. Therefore, a planet with a larger mass is able to perturb the orbits of a small body's ring particles at a greater distance than a body with a smaller mass. The intersection between 138 2D slices of the structure in Fig. 3 with constant r and 138 2D slices with constant v_∞ was examined – 46 with constant $r =$ 30 000 km, 46 with constant $r =$ 50 000 km, and 46 with constant $r =$ 100 000 km. The intersection of each 2D slice of constant v_∞ with each 2D slice of constant r revealed that the variation in R as a function of M_p could be accurately modelled by a power law of the form

$$R \sim M_p^{\gamma}. \tag{10}$$

The exponent γ ranged from 0.229 to 0.327. The maximum value of γ occurred for values of $v_\infty = 0$ km s^{-1} and $r =$ 100 000 km. The minimum value of γ occurred for values of $v_\infty = 3.9$ km s^{-1} and $r =$ 100 000 km. As an example, Table A1 gives values of γ as a function of velocity at infinity that can be used for close encounters between any giant planet and a small body with a mass equal to the mass of Pluto with ring orbital radius of 50 000 km. Fig. 4 shows the plot of our data in R–m_s–v_∞ space for a constant ring orbital radius of 50 000 km and planet mass set equal to the mass of Jupiter. Table A2 gives ring limits for close encounters between Jupiter and

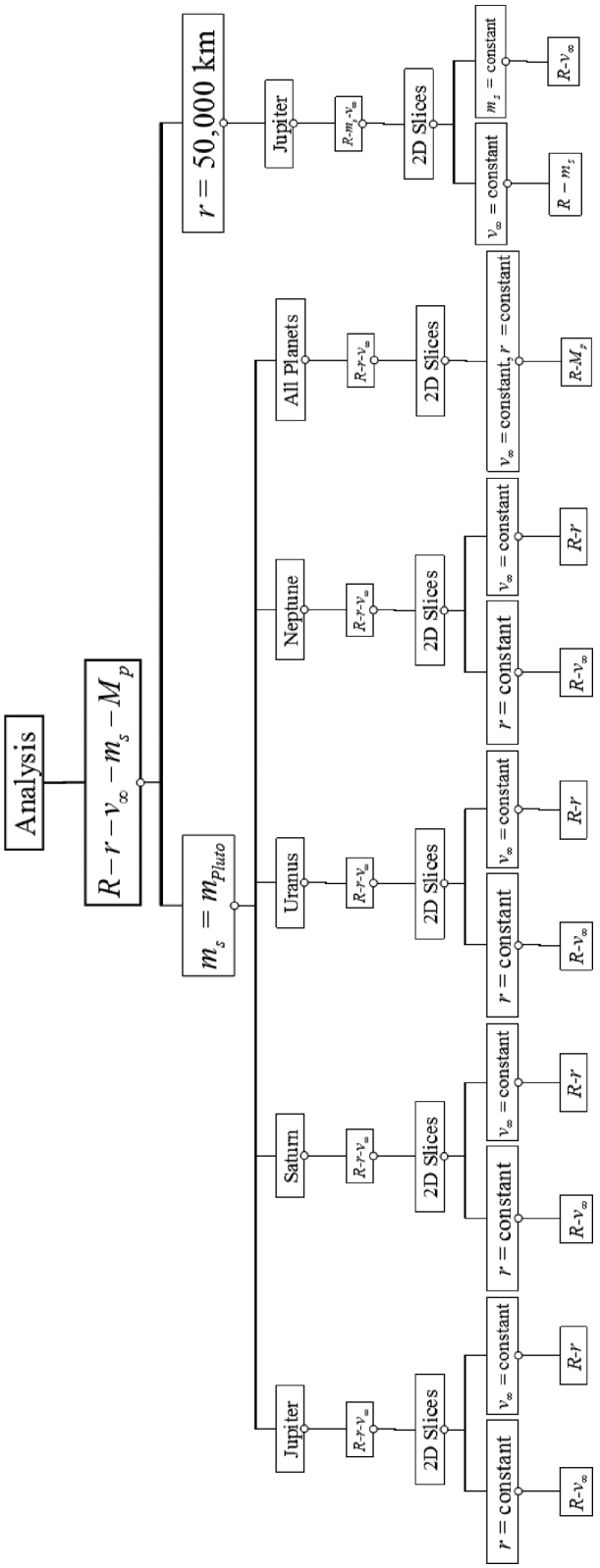

Figure 1. This map shows how the two-dimensional slices of the data are created.

a Pluto-like body with a ring orbital radius of 50 000 km for the range $0 \leq v_\infty \leq 9$ km s^{-1}.

5.2 The ring limit in two dimensions

5.2.1 The ring limit versus velocity at infinity

2D slices of R–r–v_∞ space using a constant value of r for each slice show that the mathematical relationship between R and v_∞ is too complex to fit into one form. In Fig. 5 we show a typical example of a 2D slice of R–r–v_∞ space at constant r for close encounters between the four giant planets and a Pluto-like body. The top graph is for a constant r value of 100 000 km, and the bottom for a constant r value of 30 000 km. Usually the ring limit increases with v_∞, but in the top graph R decreases with increasing v_∞ for values above 7 km s^{-1} for Uranus and 7.75 km s^{-1} for Neptune. In the bottom graph R increases with increasing v_∞ over all values. The y intercepts of graphs of this type increase with the mass of the planet. The plots for Uranus and Neptune seem to plateau at higher velocities, while those of Jupiter and Saturn less so. We speculate that the plots of Jupiter and Saturn may also plateau but at higher velocities outside the range of this study.

5.2.2 The ring limit versus ring orbital radius

2D slices of R–r–v_∞ space using a constant value of v_∞ for each slice show that R varies with r according to a power law of the form

$$R \sim r^{\alpha}, \tag{11}$$

with the exponent α varying with the value of v_∞ used for the slice. Fig. 6 shows the behaviour of α with varying v_∞. Each value of α was found from a regression on 20 data points in R–r space over a ring orbital radius range of 30 000–100 000 km while holding the velocity at infinity constant. α increases with increasing v_∞ over a range of 0–7.5 km s^{-1} and then decreases with increasing v_∞ over a range of 7.5–9 km s^{-1}. α values for close encounters between Jupiter and a Pluto-like body can be seen in Table A3.

For slices with v_∞ approaching zero (a parabolic orbit), α approaches 1.0. This means that for parabolic orbits, the ring limit varies linearly with r. Fig. 7 shows two examples of 2D slices of the ring limit versus ring orbital radius for close encounters between Jupiter and a Pluto-like body. The top slice is for a constant v_∞ of 9 km s^{-1}. The best-fitting curve is shown and corresponds to an α value of 1.15. The square regression coefficient is 0.999. The bottom slice is for a constant $v_\infty = 0.25$ km s^{-1}. The best-fitting curve is shown and corresponds to an α value of 1.0007. The square regression coefficient is 0.9999.

5.2.3 The ring limit versus small body mass

2D slices of R–m_s–v_∞ space using a constant value of v_∞ for each slice show that R varies with m_s according to a power law of the form

$$R \sim m_s^{\beta}. \tag{12}$$

One example is shown in Fig. 8 for close encounters with Jupiter for a constant $v_\infty = 0.75$ km s^{-1} and ring orbital radius = 50 000 km. In this example, $\beta = -0.3340$ and the square regression coefficient = 0.999. For any particular 2D slice of this type, β depends on the value of v_∞ used for the slice. In our data, β varies between -0.39 and -0.33 with the value approaching $-1/3$ as the velocity at infinity approaches zero. Fig. 9 shows one example of how β

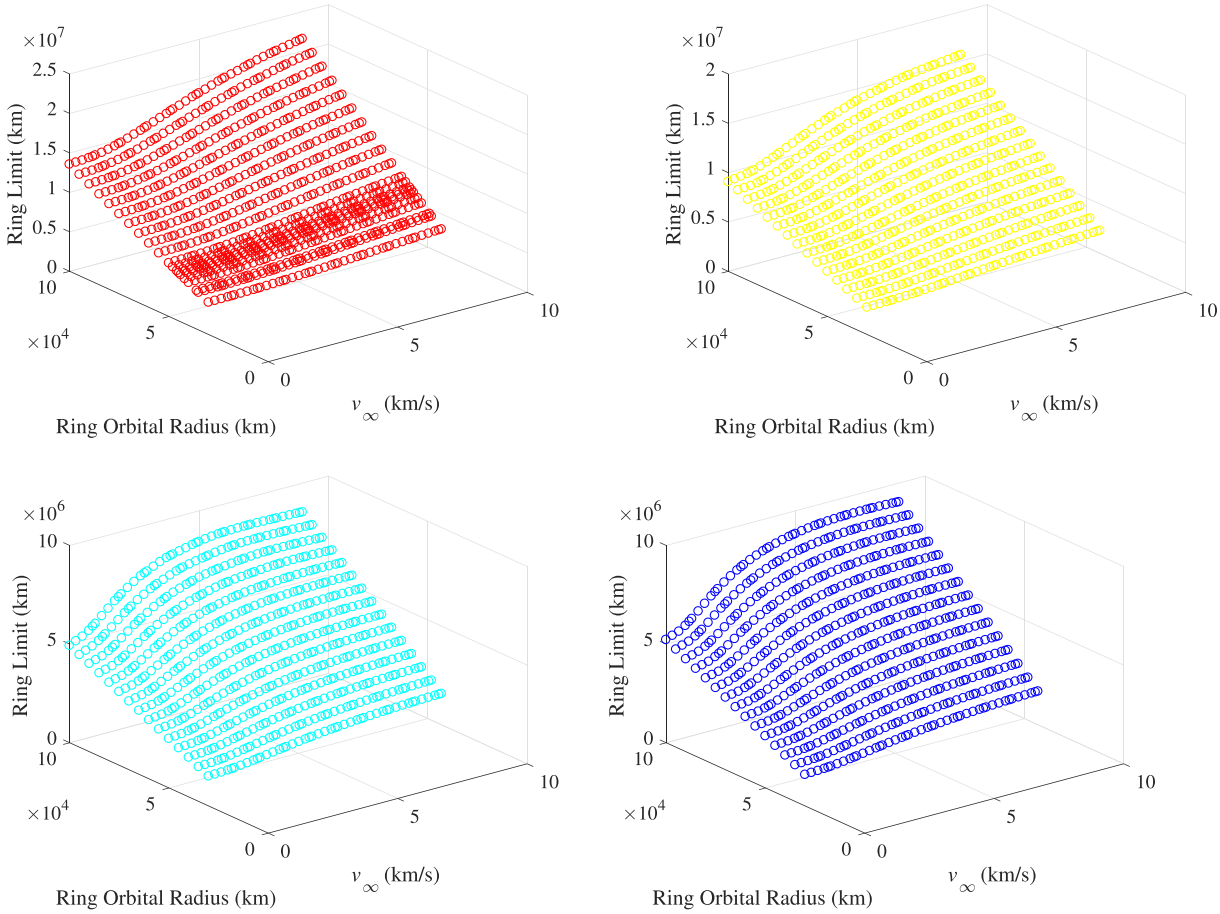

Figure 2. Plots of our data in R–r–v_∞ space for each planet for close encounters with a Pluto-like body. Jupiter's graph is to the upper left, Saturn's to the upper right, Uranus' to the lower left, and Neptune's to the lower right.

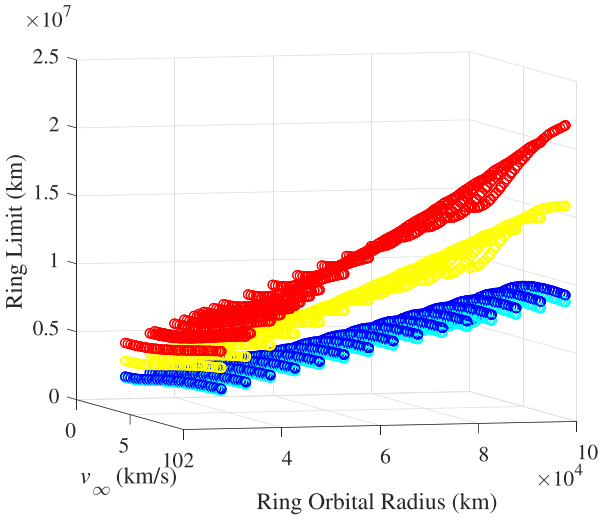

Figure 3. Plots of our data in R–r–v_∞ space colour coded by planet for close encounters with a Pluto-like body. The colours by planet are Jupiter – red, Saturn – yellow, Neptune – blue, and Uranus – cyan. (The reader is referred to the digital version for a colour image.)

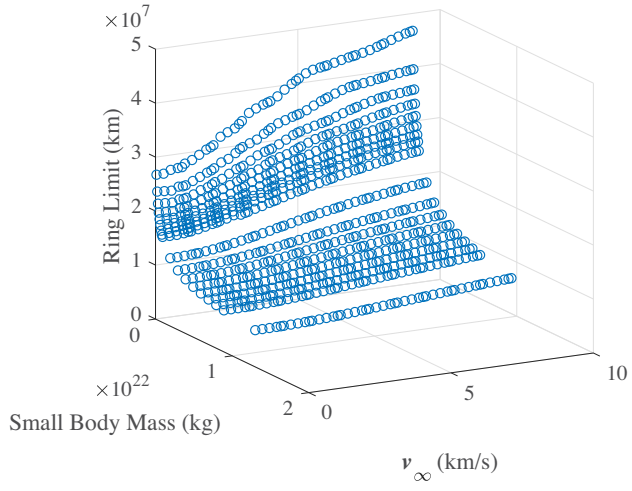

Figure 4 The plot of our data in R-m_s-v_∞ space for a constant ring orbital radius of 50,000 km and planet mass equal to the mass of Jupiter.

varies with the velocity at infinity for close encounters with Jupiter using a constant ring orbital radius of 50 000 km. Each value of β was found using regression on 18 data points in R–m_s space over a

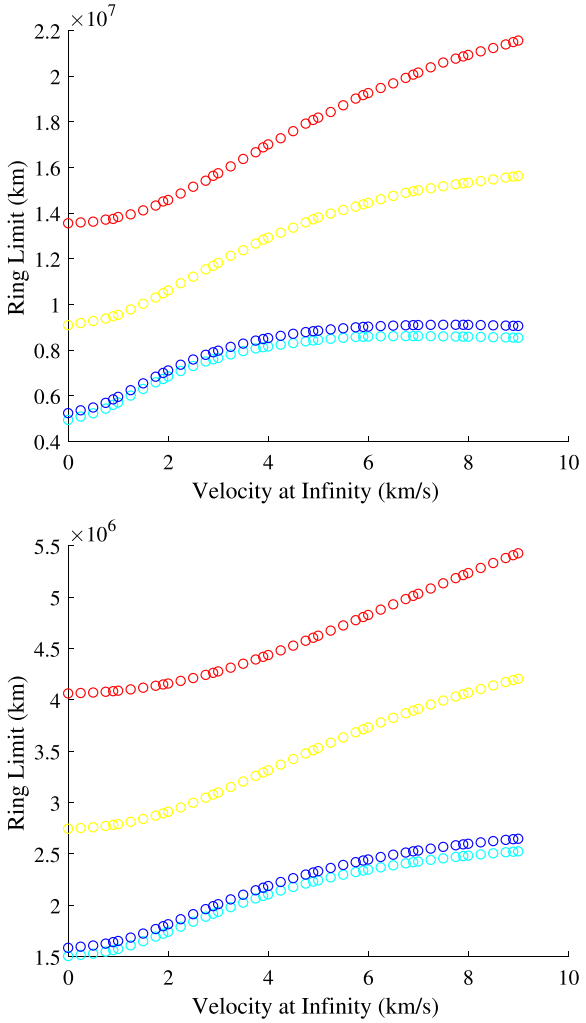

Figure 5. The ring limit as a function of velocity at infinity for a constant ring orbital radius of 100 000 km (top) and 30 000 km (bottom) for close encounters between a Pluto-like body and Jupiter (red), Saturn (yellow), Neptune (blue), and Uranus (cyan). Usually the ring limit increases with v_∞ but in the top graph R decreases with increasing v_∞ for values above 7 km s^{-1} for Uranus and 7.75 km s^{-1} for Neptune. In the bottom graph R increases with increasing v_∞ over all values. Thus, the mathematical relationship between R and v_∞ is too complex to fit into one form. The y intercepts of graphs of this type increase with the mass of the planet. (The reader is referred to the digital version for a colour image.)

mass range of 2×10^{20} kg to the mass of Pluto (1.309×10^{22} kg) while holding the velocity at infinity constant. β decreases with v_∞ over a range from 0.25 to about 5.5 km s^{-1} and increases with v_∞ over a range from 5.5 to 9 km s^{-1}. Table A4 gives values of β for close encounters between Jupiter and small bodies each with a ring orbital radius of 50 000 km.

5.2.4 The ring limit versus velocity at infinity over a range of small body masses

2D slices of R–m_s–v_∞ space using a constant value of m_s show that no particular mathematical form can be used to describe how R varies with v_∞. Slices with the highest small body masses had more well-defined plots compared to slices with the lowest masses. Two examples are shown in Fig. 10 for a constant small body mass of 2×10^{20} and 1.309×10^{22}kg (the mass of Pluto) for close encounters with Jupiter and ring orbital radius = 50 000 km. The slice associated with the Pluto-like body is best fit to an exponential function with square regression coefficient of 0.993. The slice associated with the lower mass is best fit to a linear function and has a weaker fit with a square regression coefficient of 0.966.

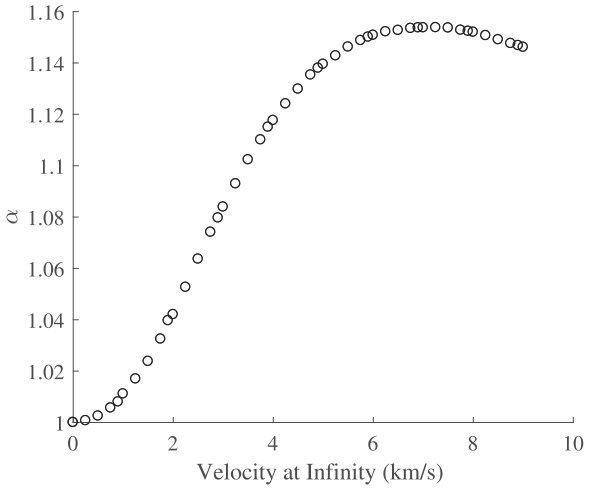

Figure 6. 2D slices of R–r–v_∞ space using a constant value of v_∞ for each slice show that the ring limit varies with ring orbital radius according to a power law of the form R–r^α with the value of α varying with the value of v_∞ used for the slice. This graph shows the best-fitting exponent, α, versus the constant value of v_∞ used for the slice for close encounters between Jupiter and a Pluto-like body. α increases with increasing v_∞ over a range of 0–7.5 km s^{-1} and then decreases with increasing v_∞ over a range of 7.5–9 km s^{-1}. Notice how as v_∞ approaches 0 (a parabolic orbit), the best-fitting exponent approaches 1.0. This means that for parabolic orbits, the ring limit varies linearly with r.

5.3 *f*, the ring limit relative to the tidal disruption distance

5.3.1 f *versus velocity at infinity*

Fig. 11 shows 20 2D slices of f versus v_∞ for 20 different values of constant r for close encounters between Jupiter and a Pluto-like body. Contours of constant ring orbital radius are colour coded. Along a contour, f increases with v_∞. Two of the contours are shown in blue as a set of data points on a smooth curve. The top contour is for a constant r= 100 000 km, and the bottom is for a constant r= 30 000 km. The higher the v_∞, the greater the range of f over all values of r. The largest value obtained by f is 2.84. As v_∞ approaches 0, all contours converge onto nearly one line, making f nearly independent of r and linear with v_∞. The y intercept for all contours is approximately $f_{\min} = 1.8$.

5.3.2 f *versus planet mass*

Graphs analogous to Fig. 11 for other planets have the same general shape but the average y intercept decreases with increasing planet mass as shown in Fig. 12. For each planet, an average y intercept was found by averaging up to 20 values of f each taken from a 2D slice of constant $v_\infty = 0$ in R–r–v_∞ space for close encounters between that giant planet and a Pluto-like body. It can be seen that the average y intercepts for the different planets all lie around 1.8.

5.3.3 f *versus ring orbital radius*

Fig. 13 shows 46 2D slices of constant v_∞ for close encounters

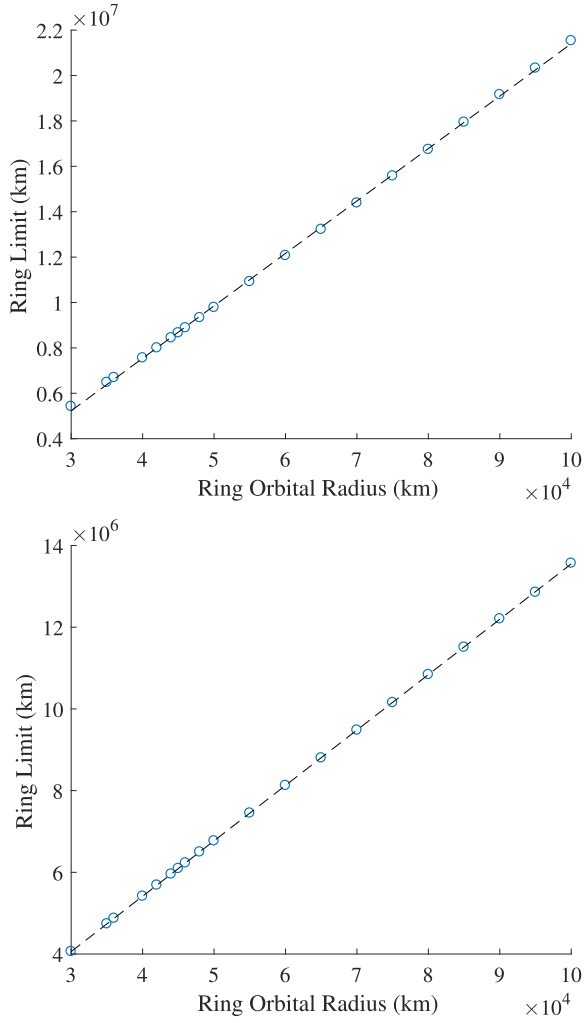

Figure 7. Top: ring limit versus ring orbital radius for a constant velocity at infinity of 9 km s^{-1} for close encounters between Jupiter and a Pluto-like body. Graphs of this type fit very well to a power law with the exponent on r approaching 1 as the velocity at infinity approaches 0 (a parabolic orbit). In this graph, the best-fitting exponent is 1.15, and the square regression coefficient is 0.999. The standard error is 0.002. Bottom: ring limit versus ring orbital radius for a constant velocity at infinity of 0.25 km s^{-1} for close encounters between Jupiter and a Pluto-like body. The exponent on r is 1.0007. The square regression coefficient is 0.9999. The standard error is 0.0005.

between Jupiter and a Pluto-like body. Contours of constant v_∞ are colour coded. Along a contour, f generally increases with r. Two contours are shown in blue as a set of data points on a smooth curve. The top contour is a curve of constant $v_\infty = 9$ km s^{-1}, and the bottom is a curve of constant $v_\infty = 0$ km s^{-1} (parabolic orbits). The value of f along the top contour increases with increasing orbital radius, however, the value of f along the bottom contour remains remarkably constant at a value around 1.8.

5.3.4 f *versus small body mass*

Fig. 14 shows 18 2D slices of constant small body mass for close encounters with Jupiter, $r = 50\,000$ km. Contours of constant v_∞ are colour coded. Along a contour, f generally decreases with m_s. Two contours are shown in blue as a set of data points on a smooth curve. The top contour is a curve of constant $v_\infty = 9$ km s^{-1}, and the bottom is a curve of constant $v_\infty = 0$ km s^{-1} (parabolic orbits). The value of f along the bottom contour remains remarkably constant at a value around 1.8. The vertically aligned set of data points on the far right is for Pluto.

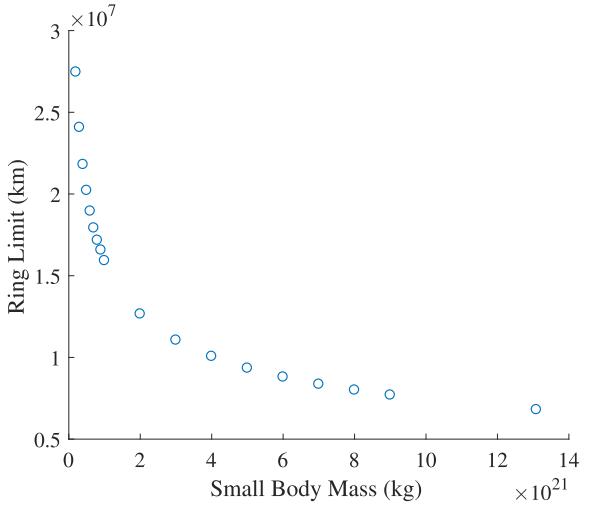

Figure 8. A 2D slice of ring limit versus small body mass for constant velocity at infinity = 0.75 km s^{-1} and constant ring orbital radius = 50 000 km for close encounters with Jupiter. The ring limit varies as a power law with the small body mass: $R \sim m_s^\beta$. In this example, $\beta = -0.3340$, and the square regression coefficient is 0.999. The standard error is 0.003.

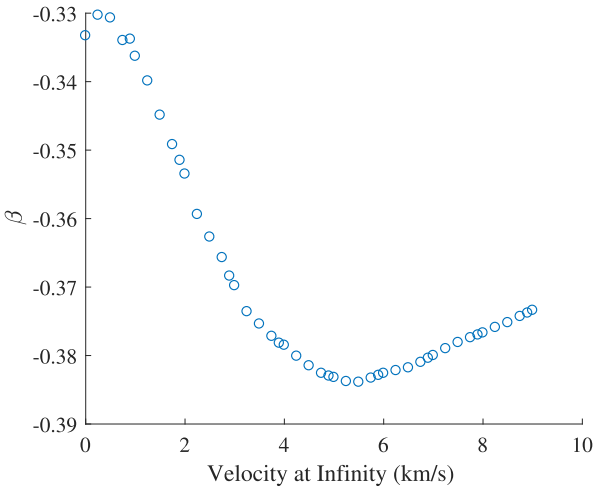

Figure 9. For 2D slices of R–m_s–v_∞ space using a constant value of v_∞ for each slice, the ring limit varies as a power law with small body mass in the form $R \sim m_s^\beta$. Values for the best-fitting exponent, β, vary with the value of the constant v_∞ used for the slice. This graph shows β versus the value of v_∞ used for the slice for close encounters with Jupiter. The ring orbital radius is held constant at 50 000 km. β decreases with v_∞ over a range from 0.25 to about 5.5 km s^{-1} and increases with v_∞ over a range from 5.5 to 9 km s^{-1}. The exponent approaches −1/3 as the velocity at infinity approaches 0.

5.4 Finding an analytical solution for the ring limit

Figs 11–14 show that the lower bound of f is approximately equal to 1.8 tidal disruption distances and is nearly independent of the mass of the planet, the ring orbital radius, and small body mass. Furthermore, Fig. 11 also shows that the ring limit equals this lower

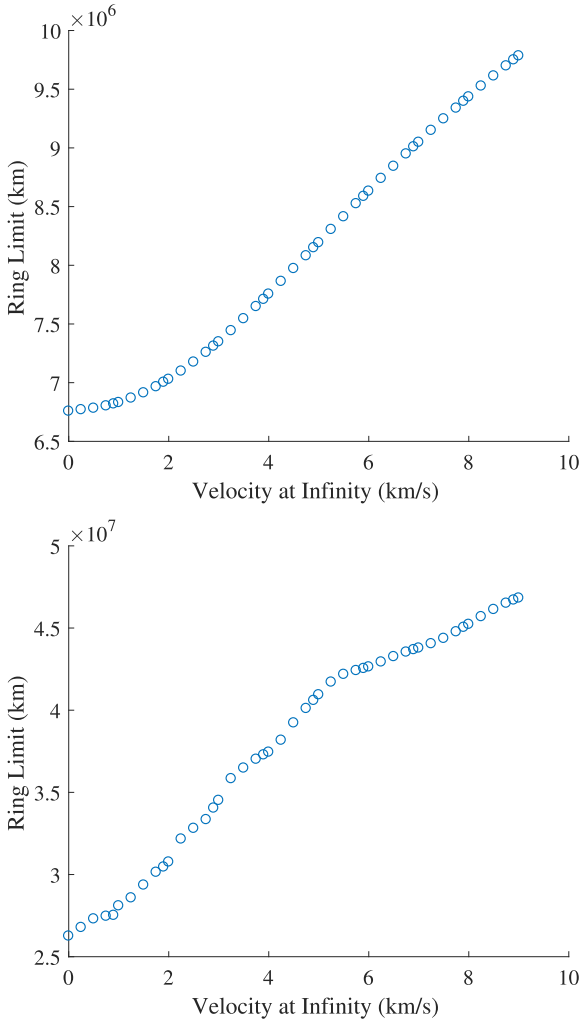

Figure 10. Top: a plot of ring limit versus velocity at infinity for a constant ring orbital radius of 50 000 km and constant small body mass equal to the mass of Pluto for close encounters with Jupiter. The best fit is exponential with a square regression coefficient of 0.993. Bottom: an analogous plot for a constant small body mass of 2×10^{20}kg. Unlike the top plot, the bottom curve is less well fit and less smooth. The best fit is linear with a square regression coefficient of 0.966.

bound only for orbits with $v_\infty = 0$ (ergo for parabolic orbits only). We now define 1.8 tidal disruption distances as the approximate distance within which all encounters between a ringed small body and a giant planet are noticeable. Thus, from equation (9), an analytical solution for the ring limit for parabolic orbits is

$$R \simeq 1.8r\left(\frac{3M_\mathrm{p}}{m_\mathrm{s}}\right)^{\frac{1}{3}}. \tag{13}$$

For hyperbolic orbits, no one mathematical form for R could be found. However, analytical solutions for the ring limit could be found for specific cases. For example, a 2D slice of constant v_∞ of the plot of our data in R–r–v_∞ space for the planet Jupiter in Fig. 2 can be analysed using regression to obtain an analytical solution for R for close encounters between Jupiter and a Pluto-like body as a function of r over the range $30\,000 \leq r \leq 100\,000$ km. The best-fitting solution for R in units of km for $v_\infty = 5$ km s^{-1} is

$$R \simeq 36.3r^{1.1395}. \tag{14}$$

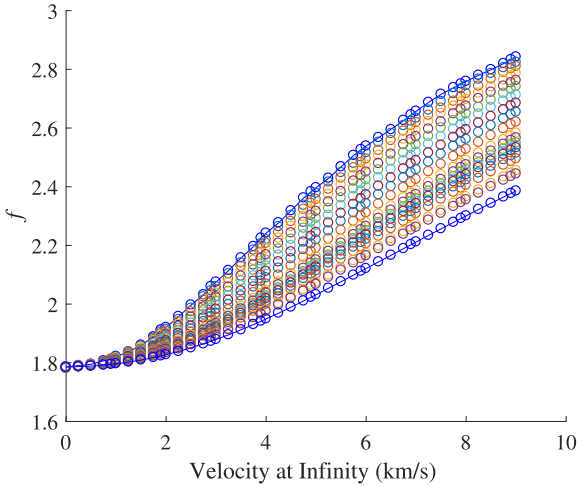

Figure 11. 20 2D slices of f versus v_∞ for 20 different values of constant r per slice for close encounters between Jupiter and a Pluto-like body. Contours of constant ring orbital radius are colour coded. Along a contour, f increases with v_∞. Two contours are shown in blue as a set of data points on a smooth curve. The top contour is for a constant r= 100 000 km, and the bottom is for a constant r= 30 000 km. The function f has a wider range for higher velocities but as v_∞ approaches 0, all contours converge onto nearly one line, making f nearly independent of r and linear with v_∞. The largest value obtained by f is 2.84. The y intercept for all contours is approximately 1.8. (The reader is referred to the digital version for a colour image.)

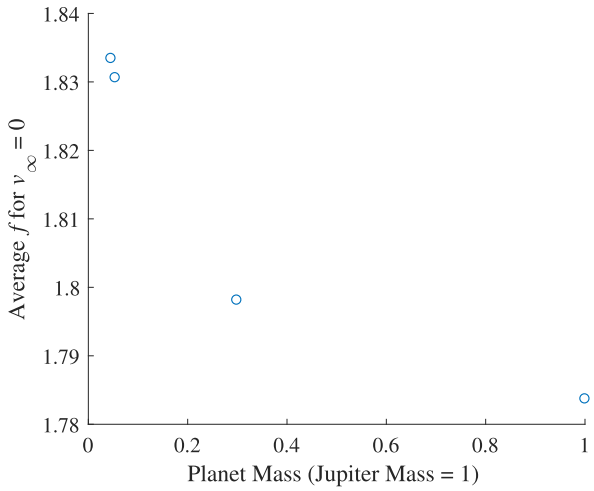

Figure 12. The average value of f for a constant $v_\infty = 0$ km s^{-1} (a parabolic orbit) for each giant planet for close encounters with a small body with the mass of Pluto. For each planet, an average f value was found by averaging all the values of f in a 2D slice of constant $v_\infty = 0$ in R–r–v_∞ space. It was decided that a range of $30\,000 \leq r \leq 100\,000$ km would be used for these simulations. Through that range, we sampled at increments of 5000 km. In addition, we performed extra simulations for Saturn (r= 25 000 km) and Jupiter (r= 36 000, 42 000, 44 000, 46 000, and 48 000 km), in order to help us better characterize the behaviour of rings for encounters with those planets. Up to 20 different ring orbital radii were used. For each planet, this average value of f corresponds to the lower bound of f and rounds off to 1.8 to two significant figures. The average value of f decreases with planet mass.

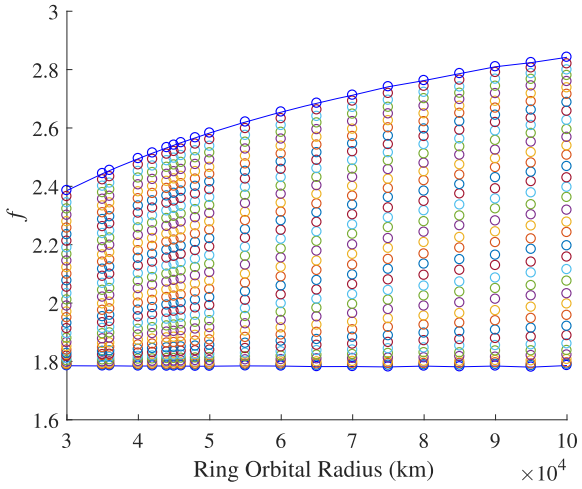

Figure 13. 46 2D slices of constant v_∞ for close encounters between Jupiter and a Pluto-like body. Contours of constant v_∞ are colour coded. Along a contour, f generally increases with r. Two contours are shown in blue as a set of data points on a smooth curve. The top contour is a curve of constant $v_\infty = 9$ km s^{-1}, and the bottom is a curve of constant $v_\infty = 0$ km s^{-1} (parabolic orbits). The value of f along the top contour increases with increasing orbital radius, however, the value of f along the bottom contour remains remarkably constant at a value around 1.8. (The reader is referred to the digital version for a colour image.)

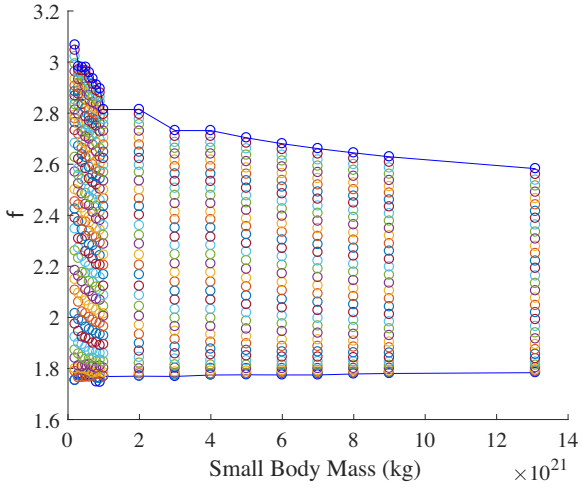

Figure 14. f versus small body mass for 18 2D slices of constant small body mass for close encounters with Jupiter, r= 50 000 km. Contours of constant v_∞ are colour coded. Along a contour, f generally decreases with m_s. Two contours are shown in blue as a set of data points on a smooth curve. The top contour is a curve of constant $v_\infty = 9$ km s^{-1}, and the bottom is a curve of constant $v_\infty = 0$ km s^{-1} (parabolic orbits). The value of f along the bottom contour remains remarkably constant at a value around 1.8. The vertically aligned set of data points on the far right is for Pluto. (The reader is referred to the digital version for a colour image.)

5.5 Applying the analytical solutions

Our analytical solutions can be used to determine ring limit values for close encounters not done in this study. As an example, suppose you wanted to know the ring limit for a small body of mass 7.986×10^{18}kg with a ring orbital radius of 50 000 km and a velocity at infinity of 7.78 km s^{-1} for a close encounter with Jupiter. Call these the target mass, target velocity, and target radius, respectively. Call the ring limit for this body $R_{\rm target}$. Here are the steps you would take.

(i) Using Table A2, find the ring limit for a Pluto-like body with a v_∞ value closest to the target v_∞. From the table, the closest v_∞ would be 7.75 km s^{-1}. Set the source mass, $m_{\rm source}$, equal to the mass of Pluto.

(ii) Use interpolation of our data in Table A2 to convert the ring limit for $v_\infty = 7.75$ km s^{-1} to a ring limit for $v_\infty = 7.78$ km s^{-1}. Call this the source ring limit, $R_{\rm source}$.

(iii) Using Table A4, find the value of the exponent on the small body mass, β, for $v_\infty = 7.75$ km s^{-1}. Use interpolation to find β for $v_\infty = 7.78$ km s^{-1}.

(iv) Use a proportion to find the ring limit for $m_s = 7.986 \times 10^{18}$kg, $R_{\rm target} = R_{\rm source}\left(\frac{m_{\rm target}}{m_{\rm source}}\right)^{\beta}$.

For close encounters with Saturn, Uranus, or Neptune, Tables A5–A7 can be used, respectively, instead of Table A2. We tested the β values to make sure that they were applicable to close encounters between small bodies and any giant planet – not just Jupiter. We accomplished this by calculating ring limits for close encounters between the other three giant planets and selected small bodies of various masses and v_∞ using two different techniques. The first technique made use of the relation $R \sim M_{\rm p}^{\gamma}$. The exponent γ was found using Table A2 for the v_∞ in question. A proportion was then used to convert ring limits for close encounters with Jupiter to ring limits for close encounters with each giant planet:

$$R_{\rm planet} = R_{\rm Jupiter}\left(\frac{M_{\rm p}}{M_{\rm Jupiter}}\right)^{\gamma}, \tag{15}$$

where $R_{\rm planet}$ is the ring limit for a close encounter between the planet and the small body in question, $R_{\rm Jupiter}$ is the ring limit for a close encounter between Jupiter and the small body in question, $M_{\rm p}$ the mass of the other planet, and $M_{\rm Jupiter}$ is the mass of Jupiter. The second technique made use of the relation $R \sim m_{\rm s}^{\beta}$. Using the second technique, the ring limit was found from Tables A5–A7 depending on the planet for the v_∞ in question. β was determined for the v_∞ in question using Table A4. A proportion was then used to convert ring limits for close encounters between the planet and Pluto to ring limits for close encounters between the planet and the small body in question:

$$R_{\rm planet} = R_{\rm Pluto}\left(\frac{m_{\rm s}}{m_{\rm Pluto}}\right)^{\beta}, \tag{16}$$

where $R_{\rm Pluto}$ is the ring limit for a close encounter between Pluto and the planet and $m_{\rm Pluto}$ is the mass of Pluto. We found good enough agreement between corresponding values found using the two techniques to warrant the use of β values to find approximate ring limits for close encounters for each of the giant planets. To test our analytical solutions, we used them to find ring limit values for close encounters between the giant planets and a fictitious Chariklo with a mass of 7.986×10^{18}kg and ring orbital radius of 50 000 km over the range $0 \leq v_\infty \leq 9$ km s^{-1}. These were then compared to $d_{\rm min}$ values reported by Araujo et al. (2016) for noticeable close encounters between giant planets and the real Chariklo with a ring orbital radius of 410 km and the same mass as our fictitious Chariklo. Each reported $d_{\rm min}$ value had a different velocity at infinity. Their system was non-planar and included the Sun, the four giant planets of the Solar system, Chariklo, and 100 massless test particles for the outer ring (effectively the seven-body problem). As their simulation was non-planar, the rings of Chariklo were not restricted to the plane

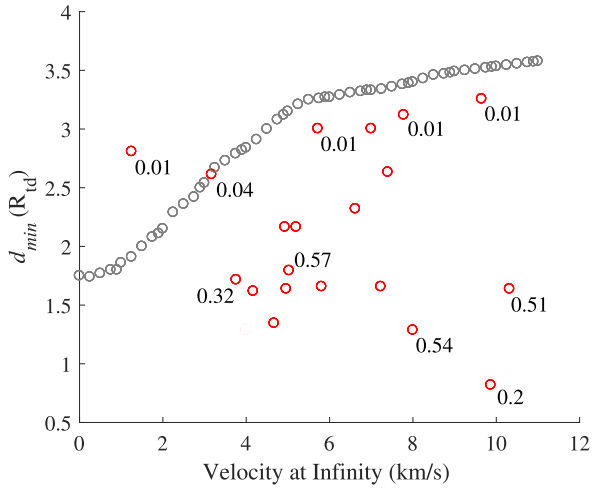

Figure 15. The $d_{\min}$ values reported by Araujo et al. (2016) and ring limit upper bound curve versus velocity at infinity for close encounters between Chariklo and Jupiter. Our analytical ring limit upper bound values are shown in grey for a fictitious Chariklo with a ring orbital radius of 50 000 km and a mass of 7.986×10^{18} kg. The $d_{\min}$ values are shown in red for a Chariklo with a ring orbital radius of 410 km and the same mass as the fictitious Chariklo. All of the close encounters are noticeable ($\Delta e_{\max} \geq 0.01$) with $\Delta e_{\max}$ ranging from 0.01 to 0.57. $\Delta e_{\max}$ values are shown for selected data points. Only one $d_{\min}$ value ($v_\infty = 1.25$ km s^{-1}, $d_{\min} = 2.81 R_{td}$) lies beyond its ring limit upper bound. At this time we cannot explain this discrepancy. (The reader is referred to the digital version for a colour image.)

of the hyperbolic or parabolic orbit about the planet as they were in our study. Since planar rings are more easily perturbed than non-planar rings, then for any noticeable close encounter with a given v_∞, the ring limit will be greater than or equal to the $d_{\min}$ value of the encounter. This reflects the fact that given all other quantities constant, a small body with inclined rings must get closer to the planet than a small body with planar rings in order for the close encounter to have a noticeable effect because when the rings are inclined, only the gravitational force component of the planet in the plane of the rings perturbs the eccentricity of the ring particle orbits (Murray & Dermott 1999). Given that f decreases with decreasing r if all other variables are constant, the ring limit for the real Chariklo with a ring orbital radius of 410 km for any particular v_∞ value will have a smaller f than the corresponding analytical value at the same v_∞ found for $r =$ 50 000 km. Thus, in this case, our analytical values form an upper bound curve on $d_{\min}$ such that the ring limit and $d_{\min}$ values for the real Chariklo will lie below the curve in $d_{\min}$–v_∞ space. The difference between the curve and the ring limit for the real Chariklo decreases with decreasing v_∞ because as Fig. 11 shows, f becomes independent of r as v_∞ approaches 0. Such a curve for close encounters between our fictitious Chariklo and Jupiter is shown in Fig. 15. The curve formed by our analytical data points is shown in grey. $d_{\min}$ values for close encounters between Jupiter and a real Chariklo with a ring orbital radius of 410 km and a mass equal to the same mass as the fictitious Chariklo reported by Araujo et al. (2016) are shown in red. To cover the full velocity range of these $d_{\min}$ values, we extrapolated our curve to extend the range to $v_\infty = 11$ km s^{-1}. 19 out of 20 $d_{\min}$ values lie below the curve as expected. The one exception lies at ($v_\infty = 1.25$ km s^{-1}, $d_{\min} = 2.81 R_{td}$). At this time we cannot explain this discrepancy. Another peculiar value lies at ($v_\infty = 3.17$ km s^{-1}, $d_{\min} = 2.61 R_{td}$). Though seemingly on our curve, it is actually $0.02 R_{td}$ below it.

We present three different ways to use this curve.

(i) Include velocity effects and set the ring limit equal to the curve so that the ring limit varies with v_∞ as has just been shown. This curve would be different for each planet.

(ii) Ignore velocity effects and set the ring limit numerically equal to the maximum value of the curve, $f_{\max}$, over the v_∞ range in question. In our case this occurs at $v_\infty = 9$ km s^{-1} This maximum value would vary with the planet mass.

(iii) Ignore velocity effects and set the ring limit equal to a constant lower bound value of 1.8 tidal disruption distances for each planet.

Each method has its own advantages and disadvantages. Including velocity effects is the most accurate method but is more complicated as each value of velocity at infinity has its own unique ring limit. This makes computations of close encounter severity more intensive and may require interpolation or extrapolation. Setting the ring limit equal to a maximum curve value for each planet is simpler but may cause some close encounters to be classified as moderate when actually they are not noticeable. As an example of using this method, consider Fig. 15. The figure shows that over the range $0 \leq v_\infty \leq 9$ km s^{-1} the curve reaches a maximum value of about $3.5 R_{td}$. Therefore, using this method, the ring limit would be set to a constant maximum value of $R = 3.5 R_{td}$ (or $f_{\max} = 3.5$) for close encounters between our fictitious Chariklo and Jupiter. This technique was repeated to obtain the $f_{\max}$ values for close encounters between Chariklo and the other giant planets. The results were $f_{\max} = 3.9$ for Saturn, $f_{\max} = 4.3$ for Uranus, and $f_{\max} = 4.2$ for Neptune. Using the second method would ensure that all close encounters subject to the condition $d_{\min} > f_{\max}$ are not noticeable. However, notice in the figure that as v_∞ approaches 0 there is a region that lies below $3.5 R_{td}$ but above the curve. Using this method, close encounters with $d_{\min}$ values in this region would be mistakenly classified as moderate. Also, shown in Fig. 15 are $\Delta e_{\max}$ values for selected close encounters. It can be seen that using our scale, even a close encounter of moderate severity can cause the change in eccentricity of a ring particle to exceed 0.5. With no correction to the test particle's orbit, it would then possibly only take two moderate close encounters to remove a ring particle from its orbit entirely. Though this may not result in the entire loss of a ring, the cumulative effect of multiple moderate encounters may not be negligible and may result in the loss of ring particles. To test our analytical $f_{\max}$ values, we compared them to experimental $d_{\min}$ values for noticeable close encounters between the real Chariklo and Saturn or Uranus reported by Araujo et al. (2016). Each $d_{\min}$ value was found to be less than its respective $f_{\max}$ value as can be seen in Table A8. Analytical $f_{\max}$ values for close encounters between each giant planet and a fictitious Chiron or Haumea with $r =$ 50 000 km and the same mass as their real body counterpart were also found. Then $f_{\max}$ values for these bodies and the fictitious Chariklo were experimentally determined via simulations. The analytical and experimental $f_{\max}$ values are compared in Table 5 and have overall good agreement. The values for Jupiter and Saturn have the best agreement differing by at most 0.5. The values for Uranus and Neptune have weaker agreement and could differ by as much as 1.4. The values for Haumea have the best agreement of the three fictitious bodies differing by at most 0.1. Because the real Haumea, Chiron, and Chariklo have ring orbital radii orders of magnitude lower than 50 000 km, any ring limit values for these real bodies will be lower than the experimental ring limit values found for our fictitious Centaurs for the reasons previously discussed. Thus, the experimental $f_{\max}$ values in Table 5 are greater than the $f_{\max}$ values of the real Haumea, Chiron, and Chariklo. For example, in Table 5 it can be seen that using the second method yields a

Table 5. Analytical and experimental ring limit upper bound maximum (f_{max}) values found using $v_\infty = 9$ km s^{-1} for close encounters between each giant planet and a fictitious Chiron, Chariklo, or Haumea with a ring orbital radius of 50 000 km. The masses used for Chiron, Chariklo, and Haumea were 2.7×10^{19}, 7.986×10^{18}, and 4.006×10^{21} kg, respectively.

Body	Planet	$f_{max\_analytical}$	$f_{max\_experimental}$
Chiron			
	Jupiter	3.3	3.0
	Saturn	3.7	3.2
	Uranus	4.1	3.0
	Neptune	4.0	3.0
Chariklo			
	Jupiter	3.5	4.0
	Saturn	3.9	3.7
	Uranus	4.3	2.9
	Neptune	4.2	3.0
Haumea			
	Jupiter	2.7	2.7
	Saturn	3.1	3.0
	Uranus	3.3	3.2
	Neptune	3.3	3.2

ring limit for close encounters between our fictitious Chariklo and Jupiter of $4R_{td}$. Therefore, the ring limit for encounters between the real Chariklo and Jupiter must be $<4R_{td}$. The same type of argument could be used for close encounters between the real Haumea, Chiron, or Chariklo and any of the four giant planets. Furthermore, over our v_∞ range 0–9 km s^{-1}, the largest value of d_{min} shown in Fig. 15 with $\Delta e_{max} = 0.01$ is $3.12R_{td}$. This means that the ring limit of the real Chariklo lies between $3.12R_{td}$ and $4R_{td}$. Our analytical value of $3.5R_{td}$ found in Table 5 for the fictitious Chariklo is close enough to that of the real body that it can actually be taken as an approximation of the ring limit of the real Chariklo. Overall, experimental f_{max} values in Table 5 for the fictitious bodies are always <4.0. This means that ring limit values for a fictitious body could be used to approximate a ring limit value for a real body with great improvement over our previously used value of $10R_{td}$. Analytical values are close enough to the experimental values to show that our analytical method can be useful in finding quick approximations of f_{max} values for real bodies without the need for time-consuming simulations.

Using the third method would ensure that all close encounters subject to the condition $d_{min} < R$ would be noticeable. The drawback with this method is that some noticeable close encounters with d_{min} above $1.8R_{td}$ but below the curve would be mistakenly counted as being not noticeable.

Using the third method, the ring limit was set to a constant 1.8 tidal disruption distances. We compared this ring limit lower bound to the 27 d_{min} values reported by Araujo et al. (2016). Fig. 16 shows those d_{min} values within $1.8R_{td}$. d_{min} values for Jupiter are in red, and the one value for Saturn in blue. Only one close encounter was severe, and there were no extreme encounters. Only 11 d_{min} values lied within $1.8R_{td}$. This means that out of the reported 27 noticeable close encounters, only 11 would be counted as noticeable using this method.

Our improved determination of the ring limit using any method showed that the ring limit was far below our initial estimate of 10 tidal disruption distances for every planet. This makes moderate close encounters less likely than the frequencies found using our previous close encounter severity scale on integrations of Chariklo and Chiron. Regardless of which method is used, the result is a more accurate measure of the value of the ring limit.

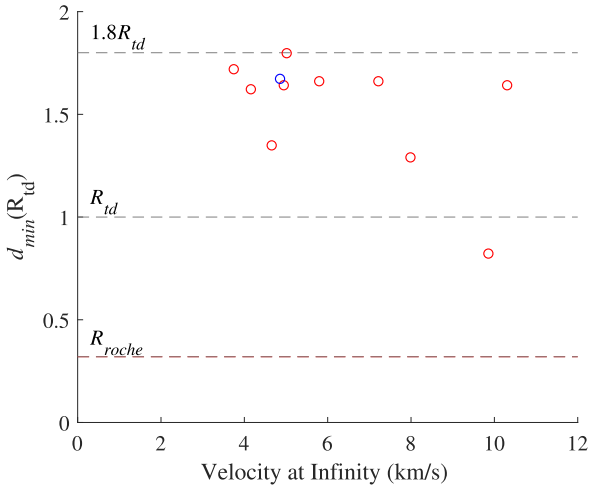

Figure 16. The d_{min} values reported by Araujo et al. (2016) within 1.8 tidal disruption distances for close encounters between Chariklo and Jupiter or Saturn. d_{min} values for close encounters with Jupiter are shown in red and those with Saturn are shown in blue. All of the close encounters are noticeable ($\Delta e_{max} \geq 0.01$) with Δe_{max} ranging from 0.2 to 0.57. The dashed lines from top to bottom are $1.8R_{td}$, R_{td}, and the Roche limits of Saturn and Jupiter. The mass and density used for Chariklo were 7.986×10^{18} kg and 970 kg m^{-3}, respectively. Out of 27 noticeable close encounters reported by Araujo et al. (2016), only 11 of these would be counted as noticeable if the ring limit is set to 1.8 tidal disruption distances. (The reader is referred to the digital version for a colour image.)

6 CONCLUSIONS

The field of ringed small bodies in the Solar system is only a few years old and started with the unexpected discovery of two narrow rings around the Centaur Chariklo. Since then, the field has been slowly growing with the discovery of rings around the dwarf planet Haumea and the potential of rings around the Centaur Chiron. Close encounters with planets are an important part of the history of ringed small bodies as they have consequences for ring origin theories and ring longevity. The severity of such an encounter depends on the mass of the small body, the mass of the planet, the inclination of the rings, the relative velocity of the small body at infinity, the initial ring orbital radius, and the minimum separation distance, d_{min} (or encounter distance). In our previous works, we studied close encounters of Chariklo and Chiron with the giant planets using numerical integration. The severity of each close encounter was found using a close encounter severity scale that we developed. In this scale, d_{min} is compared to the critical distances Hill radius, tidal disruption distance, Roche limit, and 'ring limit', R. The ring limit separates 'non-noticeable' encounters from 'noticeable' encounters. Encounters for which d_{min} is larger than the tidal disruption distance but less than the ring limit are classified as moderate encounters. Though one moderate encounter may not be strong enough to completely remove a ring, the effect of multiple moderate close encounters may result in the loss of ring particles. We define the ring limit as the d_{min} value associated with a close encounter for which the effect on the ring is just 'noticeable' for a small body in a parabolic or hyperbolic orbit about the planet in the three-body planar problem. The effect is just noticeable if the

maximum change in eccentricity of the orbit of any ring particle is 0.01. Unlike the other critical distances, the ring limit is a relatively new parameter that currently has no simple analytical expression. In our previous close encounter severity scale, the ring limit was set to a constant value of 10 tidal disruption distances for any giant planet. However, this estimate is crude and ignores the effects of the velocity at infinity. In this work, we seek to improve our close encounter severity scale by refining our expression for the ring limit so that the effects of small body mass, m_s, planet mass, M_p, velocity at infinity, v_∞, and ring orbital radius, r, are fully accounted for. Using the technique of numerical integration, close encounters between fictitious one-ringed bodies with each of the four giant planets are simulated using varying values of small body mass, ring orbital radius, and velocity at infinity. We investigate the relationship between the ring limit and each of the variables m_s, r, v_∞ and the planet mass by plotting our data in 3D R–r–v_∞ and R–m_s–v_∞ space and examining 2D slices of each with a third quantity held constant in the slice. Regression is used on a slice to determine the relationship between the ring limit and a single quantity. To find the planet mass dependence, an intersection of two slices – one of constant r and one of constant v_∞ – is used. We find that the ring limit varies as a power law with M_p, m_s, and r in the forms $R \sim M_p^\gamma$, $R \sim m_s^\beta$, and $R \sim r^\alpha$ with the exponents α, β, and γ each being a function of v_∞ and other variables. The variation of R with v_∞ did not fit any one mathematical form. The ring limit increases with increasing r and M_p but decreases with increasing m_s. For each planet, we show that the ring limit has a lower bound of approximately 1.8 tidal disruption distances (or $f_{min} = 1.8$) regardless of the mass of the small body or ring orbital radius. We find that f_{min} decreases with increasing planet mass, but we consider this dependence to be small. This means that if the encounter distance between a one-ringed small body and a planet is within $\approx$1.8 tidal disruption distances, then the close encounter always has a noticeable effect on the ring. We introduce this lower bound distance as a new critical distance for close encounters between ringed small bodies and giant planets. The ring limit equals this critical distance when the small body is in a parabolic orbit about the planet (and thus $v_\infty = 0$ by definition). Using this critical distance, an analytical solution of the ring limit for parabolic orbits is found and is approximately

$$R \simeq 1.8r\left(\frac{3M_p}{m_s}\right)^{\frac{1}{3}}. \quad (17)$$

We are unable to find a general analytical solution for R that fits all hyperbolic orbits. However, we show that analytical solutions for R can be found for specific cases. We test our results by finding analytical solutions of the ring limit for close encounters between the giant planets and a fictitious Chariklo with a ring orbital radius of r= 50 000 km and compare them to d_{min} values reported by Araujo et al. (2016) for the real Chariklo–planet encounters in the seven-body non-planar problem (Sun, Chariklo, four giant planets, and ring particle). Since the real Chariklo has a ring orbital radius two orders of magnitude lower than 50 000 km, d_{min} values for the real Chariklo are smaller than the ring limit found for our fictitious Chariklo for any velocity at infinity. We successfully show that analytical expressions can be used to find a ring limit curve in d_{min}–v_∞ space for close encounters between Jupiter and the fictitious Chariklo. We suggest three different uses for this curve: (1) use it as is and set the ring limit equal to the curve; (2) set the ring limit numerically equal to the maximum value of the curve over the v_∞ range in question ($R = f_{max}$); and (3) set the ring limit equal to a constant lower bound value of 1.8 tidal disruption distances ($R = f_{min}$). The advantage of the first method is its accuracy in determining the ring limit that varies with v_∞. The drawback is that it is more complicated to use and may involve interpolation or extrapolation. Using the first method, we find that 19 out of 20 d_{min} values for noticeable real Chariklo–Jupiter encounters reported by Araujo et al. (2016) lie within the ring limit curve as expected. We are unable to explain the one discrepancy. The second method is simpler than the first method as the ring limit is set to a value that does not vary with v_∞ but does vary with the planet. The drawback is that some close encounters of low severity lying beyond the ring limit upper bound curve but within f_{max} would be mistakenly classified as moderate encounters. Using the second method, we use analytical solutions to find f_{max} values for close encounters between each giant planet and a fictitious Chariklo, Chiron, and Haumea that each have the same mass as their real body counterpart and a ring orbital radius of 50 000 km. We then experimentally determine f_{max} values for these three bodies via direct simulation and compare them to the analytical results. We find that in each case that the experimental f_{max} values are $\leq$4.0. Since the real Chariklo, Chiron, and Haumea have ring orbital radii $\ll$50 000 km, and the ring limit decreases with decreasing ring orbital radius if other quantities are constant, the ring limit for the real Chariklo, Chiron, and Haumea must be $<4.0R_{td}$. This means that the experimental f_{max} values for the fictitious bodies can actually be used to make a much better approximation of the ring limits for their real body counterparts than the constant value of $10R_{td}$ used for R in our previous studies. When using this method, all 27 d_{min} values for noticeable encounters between the real Chariklo and Jupiter, Saturn, or Uranus reported by Araujo et al. (2016) lie below their respective f_{max} value as expected. Analytical values are close enough to the experimental values to show that our analytical method can be useful in finding quick approximations of f_{max} values for real bodies without the need for time-consuming simulations. Using the third method, we set the ring limit equal to a constant lower bound of $1.8R_{td}$. The advantage of this method is that any close encounter occurring within the ring limit would be noticeable. The drawback of this method is that some moderate close encounters occurring beyond $1.8R_{td}$ but within the ring limit upper bound curve would be mistakenly classified as non-noticeable encounters. As an example, we find that out of the 27 noticeable close encounters reported by Araujo et al. (2016), only 11 of these would be counted as noticeable with this method. In the future, it would be ideal to run further simulations to extend the phase covered by our 'standard' simulations, so that any extrapolations can begin closer to the desired outcome. Such work may also help to resolve the uncertainties in the form of the relationship between the ring limit and the various variables that can influence the final answer. In particular, it would be interesting to examine more scenarios for which v_∞ was greater than the maximum 9 km s^{-1} value used in this work to see whether the ring limit curves for Jupiter and Saturn exhibit the same behaviour as for Uranus and Neptune. As of this writing, it is not known if rings around small bodies are ubiquitous or rare. That may change in the near future with the release of the catalogue of stellar positions obtained by *Gaia*. Then, the location of the stars in the sky will become much more precisely known, which will in turn reduce the uncertainty in the path that stellar occultation event shadows will take over the Earth. That will allow more observations to be made, and since all small body rings thus far have been discovered by stellar occultation, more rings may be found. We hope that this work has laid a foundation that will be built upon and applied to other ringed bodies currently awaiting discovery.

ACKNOWLEDGEMENTS

TCH acknowledges financial support from KASI via grant #2017-1-830-03. Authors thank R. A. N. Araujo for answering their questions. They also thank the anonymous referee.

REFERENCES

Agnor Craig B., Hamilton Douglas P., 2006, Nature, 441, 192
Araujo R. A. N., Winter O. C., Prado A. F. B. A., Vieira Martins R., 2008, MNRAS, 391, 675
Araujo R. A. N., Sfair R., Winter O. C., 2016, ApJ, 824, 80
Araujo R. A. N., Galiazzo M. A., Winter O. C., Sfair R., 2018, MNRAS, 476, 5323
Bailey B. L., Malhotra R., 2009, Icarus, 203, 155
Benson A. J., Cannella C., Cole S., 2016, Comput. Astrophys. Cosmol., 3, 3
Braga-Ribas F. et al., 2014, Nature, 508, 72
Brasser R., Schwamb M. E., Lykawka P. S., Gomes R. S., 2012, MNRAS, 420, 3396
Brown M. E., Barkume K. M., Ragozzine D., Schaller E. L., 2007, Nature, 446, 294
Di Sisto R. P., Brunini A., 2007, Icarus, 190, 224
Duncan M., Levison H., Dones L., 2004, in Festou M. C., Keller H. U., Weaver H. A., eds, Comets II. Univ. Arizona Press, Tucson, AJ, p. 193
Emel'yanenko V. V., Asher D. J., Bailey M. E., 2005, MNRAS, 361, 1345
Fouchard M., Rickman H., Froeschlé Ch., Valsecchi G. B., 2014, Icarus, 231, 99
Galiazzo M. A., Wiegert P., Aljbaae S., 2016, Ap&SS, 361, 371
Groussin O., Lamy P., Jorda L., 2004, A&A, 413, 1163
Horner J., Evans N. Wyn, 2006, MNRAS, 367, L20
Horner J., Jones B. W., 2010, Astron. Geophys., 51, 6.16
Horner J., Lykawka P. S., 2010a, MNRAS, 402, 13
Horner J., Lykawka P. S., 2010b, MNRAS, 405, 49
Horner J., Wittenmyer R., 2018, Am. Astron. Soc. Meeting Abstr., 231, 128.04
Horner J., Evans N. W., Bailey M. E., 2004a, MNRAS, 354, 798
Horner J., Evans N. W., Bailey M. E., 2004b, MNRAS, 355, 321
Horner J., Lykawka P. S., Bannister M. T., Francis P., 2012a, MNRAS, 422, 2145
Horner J., Müller T. G., Lykawka P. S., 2012b, MNRAS, 423, 2587
Hyodo R., Charnoz S., Genda H., Ohtsuki K., 2016, ApJ, 828, L8
Jeans J. H., 1928, Astronomy and Cosmogony. Cambridge Univ. Press, Cambridge
Jeffreys H., 1947, MNRAS, 107, 260
Kowal C. T., Liller W., Marsden B. G., 1979, in Duncombe R. L., ed., Proc. IAU Symp. 81, Dynamics of the Solar System. Reidel, Dordrecht, p. 245
Lacerda P., Jewitt D. C., 2007, AJ, 133, 1393
Leiva R., et al., 2017, AJ, 154, 159
Levison H. F., Duncan M. J., 1997, Icarus, 127, 13
Lykawka P. S., Horner J., Mukai T., Nakamura A. M., 2012, MNRAS, 421, 1331
Meech K. J., Svoren J., 2004, in Festou M. C., Keller H. U., Weaver H. A., eds, Comets II. Univ. Arizona Press, Tucson, AJ, p. 317
Murray C. D., Dermott S. F., 1999, Solar System Dynamics. Cambridge Univ. Press, Cambridge
Napier W. M., 2015, MNRAS, 448, 27
Ortiz J. L. et al., 2015, A&A, 576, A18
Ortiz J. L., et al., 2017, Nature, 550, 219
Pan M., Wu Y., 2016, ApJ, 821, 18
Philpott C. M., Hamilton D. P., Agnor C. B., 2010, Icarus, 208, 824
Rabinowitz D. L., Barkume K., Brown M. E., Roe H., Schwartz M., Tourtellotte S., Trujillo C., 2006, ApJ, 639, 1238
Ragozzine D., Brown M. E., 2009, AJ, 137, 4766
Rawal J. J., Nikouravan B., 2011, Int. J. Fundamental Phys. Sci. (IJFPS), 1, 6
Rein H., Liu S.-F., 2012, A&A, 537, A128
Rein H., Spiegel D. S., 2015, MNRAS, 446, 1424
Sheppard S., Jewitt D., Trujillo C., Brown M., Ashley M., 2000, AJ, 120, 2687
Sicardy B., El Moutamid M., Quillen A. C., Schenk P. M., Showalter M. R., Walsh K., 2016, preprint (arXiv:1612.03321)
Sykes M. V., Walker R. G., 1991, Science, 251, 777
Tiscareno M., Malhotra R., 2003, AJ, 126, 3122
Volk K., Malhotra R., 2008, ApJ, 687, 714
Wang L., Spurzem R., Aarseth S., Nitadori K., Berczik P., Kouwenhoven M. B. N., Naab T., 2015, MNRAS, 450, 4070
Wood J., Horner J., Hinse T. C., Marsden S. C., 2017, AJ, 153, 245
Wood J., Horner J., Hinse T. C., Marsden S. C., 2018, AJ, 155, 2

SUPPORTING INFORMATION

Supplementary data are available at *MNRAS* online.

Please note: Oxford University Press is not responsible for the content or functionality of any supporting materials supplied by the authors. Any queries (other than missing material) should be directed to the corresponding author for the article.

This paper has been typeset from a TEX/LATEX file prepared by the author.